SAND2015-11007C

A Comprehensive Aero-Hydro-Structural Analysis of a 5-MW Offshore Wind Turbine System: Towards Cost-Effective Deployment of Offshore Wind Turbines in Maryland

Scott Smith[§], Abdul-Bari Syed[†], Kan Liu[‡], Daming Chen[+], Meilin Yu[*], and Weidong Zhu[#]
Department of Mechanical Engineering
University of Maryland, Baltimore County (UMBC), Baltimore, MD 21250

Rong Liu[§§]
School of Mechanical Engineering
Hangzhou Dianzi University, Hangzhou, Zhejiang, China, 310018

Mohamed Sherif Aggour[††]
Department of Civil & Environmental Engineering
University of Maryland, College Park, MD 20742

To facilitate the deployment of offshore wind turbines in Maryland wind energy area, a comprehensive aero-hydro-structural analysis is conducted for a 5-MW offshore wind turbine system. The soil-foundation interaction under complex aero-hydro loading is analyzed to provide a suitable foundation design with a high safety factor and minimal cost per unit energy. Considering the wind turbine size and hydrological characteristics, the mono-pile foundation design is selected for current study. Both the aerodynamic loading for the 5-MW wind turbine rotor defined by National Renewable Energy Laboratory (NREL), and the hydrodynamic loading on the foundations are simulated under different flow conditions using high-fidelity computational fluid dynamics (CFD) methods. The structural analyses are then carried out to estimate the safety factor of the foundation and the soil stress. Results from the synergistic analyses indicate that the current foundation design can effectively resist the aero-hydro loading. The same analysis strategy can be directly applied to other types of foundation designs.

I. Introduction

Towards the goal that 20% of Maryland's electricity be generated from renewable resources by

[§] Graduate Student, Department of Mechanical Engineering
[†] Graduate Student, Department of Mechanical Engineering
[‡] Graduate Student, Department of Mechanical Engineering
[+] Graduate Student, Department of Mechanical Engineering
[*] Assistant Professor, Department of Mechanical Engineering, AIAA Member, email: mlyu@umbc.edu
[#] Professor, Department of Mechanical Engineering, email: wzhu@umbc.edu
[§§] Associate Professor, School of Mechanical Engineering
[††] Professor, Department of Civil & Environmental Engineering

2022, the Maryland Offshore Wind Energy Act of 2013 creates a mechanism to incentivize the development of up to 500 MW of offshore wind capacity. Compared with onshore wind turbines, offshore wind turbine deployment has relaxed constraints from transportation, installation, transmission, noise reduction, and aesthetics, and enjoys generally faster and more uniform wind field at sea than on land. However, these advantages are accompanied by higher investments and more severe environmental conditions [1, 2]. Selecting the optimum design for Maryland wind farm foundations is critical because this element can represent about 20% of the total project cost [3, 4].

Although numerous onshore wind turbine structures have been constructed and the structures have had few failures occurring on the foundations [5], this may not be the case for offshore wind turbine foundations that are installed on saturated soil, where foundation failures can occur [6]. The foundations are subjected to soil-foundation interaction and more complicated dynamic loads that originated from waves, currents, winds, ice, earthquakes, and even ship impacts, which can lead to failure. While over-designing an offshore wind turbine foundation for high strength can guarantee safety of the structure, the cost would be greatly increased. To balance the construction cost and safety of an offshore wind turbine, a reliable safety evaluation becomes necessary in the foundation design. In current study, we are exploring optimal foundation design with a high safety factor and minimal cost per unit energy for deployment of offshore wind turbines in Maryland by judiciously considering effects of aero-hydro loads and seabed soil.

In state-of-the-art offshore wind turbine design tools, the aerodynamic loading is usually calculated using the blade element momentum (BEM) theory [7] or the generalized dynamic wake (GDW) theory [8]. These models are easy to implement and fast to execute. Therefore, they are very attractive to industrial design purpose. However, it has been widely recognized that these design tools cannot adequately resolve the system response to unsteady non-linear wind loading due to the simplified modeling of some critical physical processes [9, 10, 11, 12]. These processes include, but are not limited to, rotor wake rotation, dynamic stall, blade-vortex interaction, and three-dimensional (3D) turbulent flow over complex blade geometries. Therefore, there is a need of advanced computational and experimental tools to verify the results from current models, and provide insights into richer physics to guide the development of more advanced models [13, 14, 15].

Waves and currents exert periodic loads on the submerged foundations of offshore wind turbines. The calculation of wave loads on offshore structures is a challenging task involving different wave models selection, load-calculation methods and probability analyses. As mentioned previously, in state-of-the-art offshore wind turbine design tools, the hydrodynamic loading is usually evaluated based on the linear potential flow, wave theories and the semi-empirical Morison's equations [16]. These simplified physical models cannot adequately capture the system response to unsteady non-linear wave-current loading on the foundation [17, 18], e.g., second-order and high-order hydrodynamic effects, breaking waves, etc. It is desirable that high-fidelity CFD simulations can be adopted to capture these unsteady, critical physical processes. The current work will focus on free surface water flow simulation using high-fidelity CFD methods, numerical wave generation and analyses of wave loads effects on the mono-pile foundation, which is widely used to support the offshore wind turbine at water depth less than 30m.

The main design safety concerns of a pile-type foundation of an offshore wind turbine are its failure modes caused by vertical and lateral loads [19]. Vertical failure modes of such a foundation include buckling of piles and shear failure of soil surrounding piles. Lateral failure modes may depend on pile slenderness and load capacities of the pile and soil surrounding it [20]. For a foundation with

short-oversized piles, failures occur when lateral soil pressure on a pile exceeds the soil ultimate lateral resistance along the embedded pile length, and it results in rigid body rotations of the pile [21]. For a foundation with slender piles, failures occur when the bending load capacity of the pile is exceeded. To predict these failures, effects of soil-foundation interaction are critical and must be considered in associated models. There are various modeling methods for soil-foundation interaction, such as the elasticity analysis method, ultimate subgrade reaction method, elastic subgrade reaction method, and p-y curve method [22, 23, 24, 25]. However, these approaches may be erroneous for dynamic response calculations. Continuum approaches can yield more accurate results, by which dynamic stiffness and damping of soil-foundation systems are formed. These approaches treat soil surrounding a pile as a stack of independent infinitesimally thin slices, and each layer behaves under plane-strain conditions. Analytical approximate expressions of dynamic stiffness and damping of piles were developed [22], and further improved by including inertial effects of pile mass [26]. For these reasons, continuum modeling approaches are used in the current project for soil-foundation interaction.

The remainder of the paper is organized as follows. In Section II, the numerical methods and simulation parameters for aerodynamic, hydrodynamic and structural simulation will be introduced. Simulation results and discussions are then presented in Section III. Section IV concludes the paper.

II. Numerical methods and simulation parameters

The aerodynamic and hydrodynamic simulations are carried out using the commercial software ANSYS Fluent. The structural analysis is performed using the commercial software ABAQUS. Detailed numerical setup is introduced as follows.

A. Aerodynamics of the 5-MW offshore wind turbine

A.1. Wind turbine rotor geometry and mesh generation

As a first step, the 5MW wind turbine rotor geometry definition from NREL [27] is used to model the 3D rotor. The blade surfaces are assumed to be a collection of various airfoil shapes which are lofted in spanwise direction. The geometry of the rotor blade considered in this study is based on the NREL 5MW offshore baseline wind turbine described in Ref. [27]. The blade geometry data taken from the reference are summarized in Table 1. The blade is attached to the hub which gives the total rotor radius of 62.9m. The blades are twisted to enhance the aerodynamic performance.

To generate the volume mesh for the three bladed rotors, a 120° periodic domain approach is used by taking the advantage of rotational symmetry problem which can reduce the computational cost. This mesh comprises of approximately 8.9 million elements with fine resolution near the rotor surface for better capturing of flow physics, as shown in Figure 2.

To define a mesh with good resolution of critical flow features, it is important to understand the importance of boundary layer resolution. Several cases are run to gain a good understanding of the effects of improper resolution on the performance characteristics of the wind turbine. Finally, inflation layers were incorporated at the turbine blade surfaces to better resolve the boundary layer flow. Figure 3(a) presents a blade cross section view, demonstrating the high level of refinement near the blade surface with even finer resolution at the leading and trailing edges to better capture flow physics. Figure 3(b) provides a detailed view of the mesh at the leading edge. This mesh incorporates twenty inflation layers with a growth rate of 1.2. Growth rate is used to provide a variable thickness to the boundary mesh layers. This aids in capturing flow physics in the turbulent boundary layer occurring

over the blade surface. Since the boundary layer is resolved adequately, the phenomenon of separated flow features can be captured with a higher level of accuracy. However, as we move downstream in the domain there is no need for a fine resolution of elements in the domain. Hence a higher growth rate is specified there.

Table 1. Wind turbine rotor geometry definition from Ref. [27].

RNodes (m)	AeroTwst (deg.)	Chord (m)	AeroCent (−)	AeroOrig (−)	Airfoil
2.0000	0.000	3.542	0.2500	0.50	Cylinder
2.8667	0.000	3.542	0.2500	0.50	Cylinder
5.6000	0.000	3.854	0.2218	0.44	Cylinder
8.3333	0.000	4.167	0.1883	0.38	Cylinder
11.7500	13.308	4.557	0.1465	0.30	DU40
15.8500	11.480	4.652	0.1250	0.25	DU35
19.9500	10.162	4.458	0.1250	0.25	DU35
24.0500	9.011	4.249	0.1250	0.25	DU30
28.1500	7.795	4.007	0.1250	0.25	DU25
32.2500	6.544	3.748	0.1250	0.25	DU25
36.3500	5.361	3.502	0.1250	0.25	DU21
40.4500	4.188	3.256	0.1250	0.25	DU21
44.5500	3.125	3.010	0.1250	0.25	NACA64
48.6500	2.310	2.764	0.1250	0.25	NACA64
52.7500	1.526	2.518	0.1250	0.25	NACA64
56.1667	0.863	2.313	0.1250	0.25	NACA64
58.9000	0.370	2.086	0.1250	0.25	NACA64
61.6333	0.106	1.419	0.1250	0.25	NACA64
62.9000	0.000	0.700	0.1250	0.25	NACA64

Figure 1. 3D blade geometry of the 5MW wind turbine rotor.

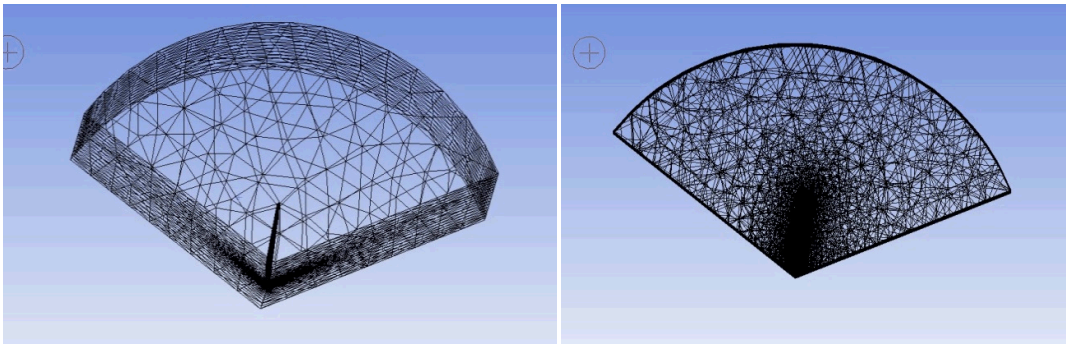

(a) (b)

Figure 2. (a) Surface grids and (b) volume grids of the computational domain for aerodynamic simulation.

Due to the size limitations and the intricacy of the flow physics, it is difficult to reduce the total number of elements in the domain in order to further decrease computational cost. After having performed three independence mesh studies (parameters given in Table 2.), mesh III is chosen for the analysis which provides better boundary layer flow physics.

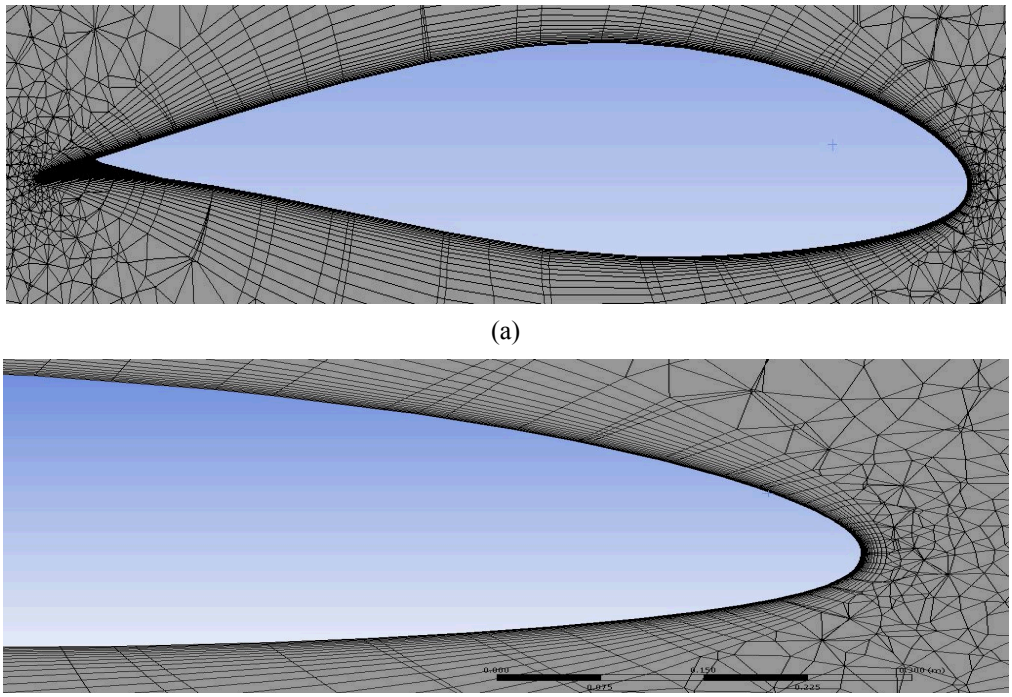

(a)

(b)

Figure 3. (a) A detailed view of meshes around a blade cross section; and (b) a detailed view of meshes near the leading edge.

Table 2. Parameters used for mesh independence study

Mesh Name	Total no. of elements
Mesh I	~2 million
Mesh II	~4.8 million
Mesh III	~8.9 million

A.2. Numerical setup

The wind speed is chosen the range of 5 m/s ~ 15 m/s, and the rotor speed sits in the range of 1 rad/s ~ 3 rad/s. The air properties at standard sea-level conditions are used. The boundary conditions are summarized in Figure 4. Specifically, the inlet boundary is set as wind velocity with velocity magnitude of 9m/s and the outlet boundary is set as pressure-outlet. The far-field is also set as velocity inlet. The left and right boundaries as shown in Figure 2 are set as rotationally periodic boundary condition. Specifically, if the rotation axis is the z-axis, then the velocities on the rotationally periodic boundaries with angle θ satisfy

$$\begin{pmatrix} u_2 \\ v_2 \\ w_2 \end{pmatrix} = \begin{pmatrix} cos\theta & -sin\theta & 0 \\ sin\theta & cos\theta & 0 \\ 0 & 0 & 1 \end{pmatrix} \begin{pmatrix} u_1 \\ v_1 \\ w_1 \end{pmatrix}. \quad (1)$$

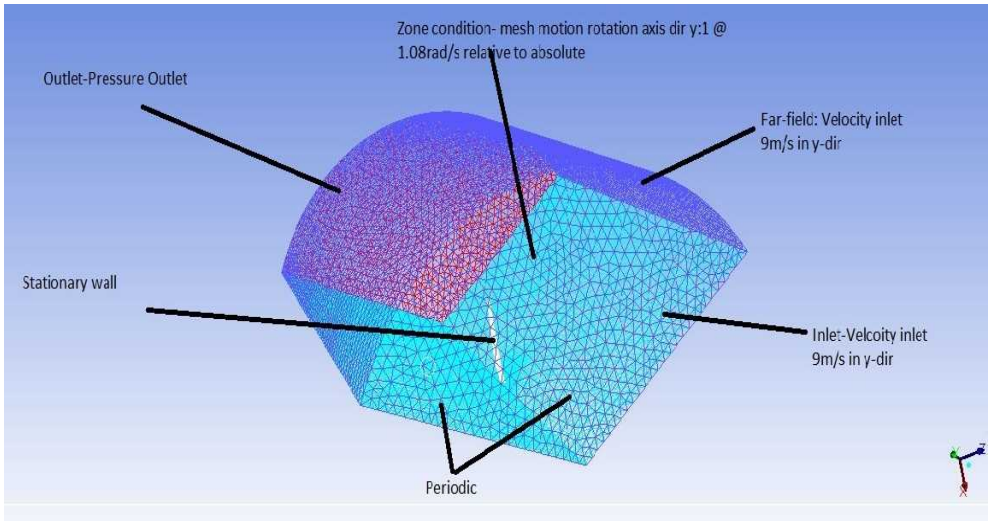

Figure 4. Boundary condition definitions for the domain.

As mentioned earlier, the Spalart-Allmaras (S-A) one-equation turbulence model is adopted in all numerical simulations. For the pressure velocity coupling, the SIMPLE algorithm is used which uses a relationship between pressure and velocity corrections to enforce mass conservation and to obtain the pressure field. This is a standard practice undertaken in order to obtain quicker yet accurate results. Residuals are set to $1 \cdot 10^{-5}$ for better convergence. A second-order implicit temporal discretization algorithm is used for time marching. The time step is set as 0.01s through a time refinement study. Table 3 summarizes the parameter setup of the current numerical simulation.

Table 3. List of input parameters in ANSYS FLUENT

Input Variable	**Value/Setting**
Model	Spalart-Allmaras (S-A)
Angular Velocity	1.08rad/s
Inlet	Velocity inlet at 9m/s
Outlet	Pressure Outlet
Far-Field	Velocity inlet at 9m/s
Pressure Velocity Coupling	SIMPLE
Discretization Scheme	Second Order Upwind
Residuals	$1 \cdot 10^{-5}$

B. Hydrodynamics of the mono-pile foundation

Wave is generated with the intrinsic wave theory in the ANSYS Fluent software under the open channel condition. In the current study, to accommodate different wave heights and periods for the Maryland offshore wind energy leasing area, the Stokes wave theory is adopted. It is a finite amplitude wave theory in inviscid fluid and irrotational motion, which was first derived by Stokes in 1847 [28]. Another wave theory suitable for the current study is the cnoidal wave theory proposed by Korteweg de Vries in 1895 [29]. In this simulation, the Stokes wave theory are chosen because of the Ursell number (i.e., $Ur=HL^2/d^3$) of all cases is smaller than 40. As illustrated in Figure 5, when the Usresll number is below 40, the errors in the predicted instantaneous discharges under wave crests from the Stokes wave theory are smaller than those from the cnoidal wave theory.

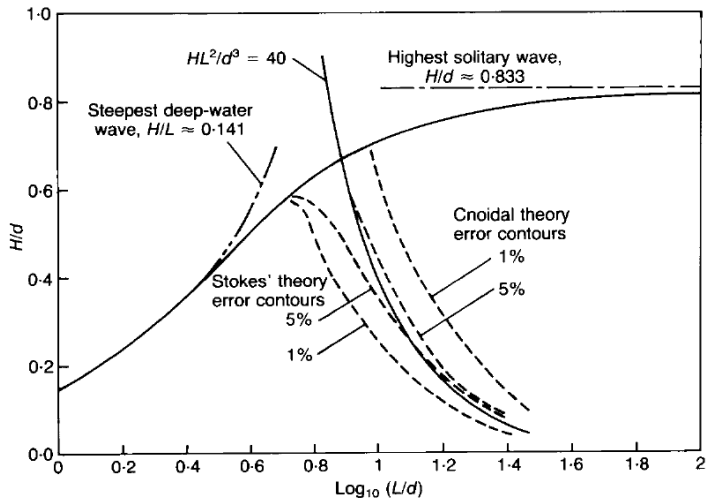

Figure 5. Contours of the errors in predicting instantaneous discharges under wave crests, together with proposed demarcation line between Stokes' and cnoidal theories. See Ref. [30].

In this numerical study, the wave height is specified in the range of 0.5 m ~ 7.8 m which is read from the chart of significant wave height from 1986 to 2008 in Delaware Bay (Note that the data are from the website of National Oceanic and Atmospheric Administration's National Data Buoy Center). Specifically, three values, namely 1 m, 4m and 7 m wave height are used to characterize the wave height conditions of the Maryland offshore wind energy leasing area. The wave period is set in the range of 2.5 s ~ 14 s with an average value of 5s. The wave length is changed to control the wave period. The wave speed is calculated in Fluent based on the flow velocity and the water depth. The flow velocity is chosen as 3 m/s, which is greater than most ocean currents in the world. Additionally, the ocean surface current in Maryland region is usually smaller than 1m/s based on the data provided on NASA's website [31]. Therefore, the current simulation is deemed as a conservative evaluation of the hydrodynamic load on the offshore wind turbine foundation.

From Table 4, the wave length and wave period are shown under different wave height conditions. No wave break will occur according to the relative depth check and wave steepness check. The wave is generated by the fifth order Stokes wave theory, which satisfies the Ursell number limit [30].

The volume of fluid (VOF) multiphase model in ANSYS Fluent is used to determine the free surface water flow. Specifically, the two phases are defined by a volume fraction for each phase. A water volume fraction value of 1 represents water and a value of 0 represents air. The fractions of air and water are defined using the step function,

$$AirFraction = step(z - z_{level}),$$
$$WaterFraction = 1 - AirFraction. \quad (1)$$

Herein, z is the height in the computational domain, and z_{level} is the height of the sea level.

A mono-pile of 60m height with 10m above the water, 20m beneath water, and 30m embedded in the soil is used in the current study. Note that the averaged water depth in Maryland offshore wind energy area is around 23m. A computational domain of about 2 million elements is generated with fine resolution near the mono-pile. The inlet boundary is set as a wave superimposed on a fixed uniform velocity. The uniform flow velocity is 3m/s which has been mentioned previously. All simulations are performed using the second-order accurate RANS simulation with the $k-\omega$

turbulence model.

Wave height (m)	1	4	7
Wave length (m)	64.0000	65.5500	68.7500
Wave period (s)	4.9945	5.0001	4.9984
Relative depth check	Min=0.0000 < H/h = 0.0500 < Max=0.7500	Min=0.0000 < H/h = 0.2000 < Max=0.7500	Min=0.0000 < H/h = 0.3500 < Max=0.7500
Wave Steepness check	Min=0.0156 < H/L = 0.0500 < Max=0.1365	Min=0.0156 < H/L = 0.0610 < Max=0.1365	Min=0.0156 < H/L = 0.1018 < Max=0.1365
Ursell Number check	Min=0.0000 < Ur = 0.5120 < Max=26.0000	Min=0.0000 < Ur = 2.1484 < Max=26.0000	Min=0.0000 < Ur = 4.1537 < Max=26.0000
Wave regime check	Min=0.0600 < h/L = 0.3125 < Max=26.0000	Min=0.0600 < h/L = 0.3051 < Max=26.0000	Min=0.0600 < h/L = 0.2909 < Max=26.0000

Table 4. Wave parameters in the current simulation.

C. Soil-foundation interaction

Continuum modeling approaches are used in the current project for structure-foundation interaction. To reduce the computational costs of continuum modeling dampers are attached at the boundary of the soil to absorb any wave propagation through the soil. Three dampers are applied at each boundary node of the continuum, the damping values are given as [32]:

$$C_{\perp} = \rho V_c A, \qquad C_{\parallel} = \rho V_s A, \tag{2}$$

where $C_{\perp}$ is the damping value of the damper normal to the surface, $C_{\parallel}$ is the damping value of the dampers parallel to the surface, ρ is the density of the soil, A is the tributary area of the surface node, V_c is the compressive wave velocity, and V_s is the shear wave velocity of the soil. The wave velocities can be obtained from the modulus of elasticity E, Poison's ratio μ, and the density of the material, as [33]:

$$V_c = \sqrt{\frac{E(1-\mu)}{\rho(1+\mu)(1-2\mu)}}, \qquad V_s = \sqrt{\frac{E}{2\rho(1+\mu)}}. \tag{3}$$

A model of a mono-pile foundation was created with a soil continuum, turbine tower, and turbine nacelle and blades was created, as shown in Figure 6. The model is the NREL 5-MW reference wind turbine and mono-pile foundation. The soil surrounding the monopole is a $60 \times 60 \times 80\, m$ solid continuum with a modulus of elasticity of 55.046 MPa, Poison's ratio of 0.35, density of $1019.4\ kg/m^3$, and 5% material damping. The SSI is modeled using the friction angels method to determine the friction coefficient; the friction angels ϕ are: 33° for the top $5\, m$, 35° for the middle $14\, m$, and 38.5° for the bottom $66\, m$. The friction coefficient between foundation and the soil is defined as [34]:

$$\nu = tan\left(\frac{2\phi}{3}\right) \tag{4}$$

The model was simulated under dynamic loads; the resulting aerodynamic loads from the aerodynamic section were applied to the model at the center point on the back of the hub. The hydrodynamic loads are modeled as the Morison equation [35] and hydrodynamic load from the CFD

wave simulation. The dynamic response is calculated using ABAQUS 6.9EF dynamic, implicit step for 20 seconds with a maximum step size of 0.5 seconds.

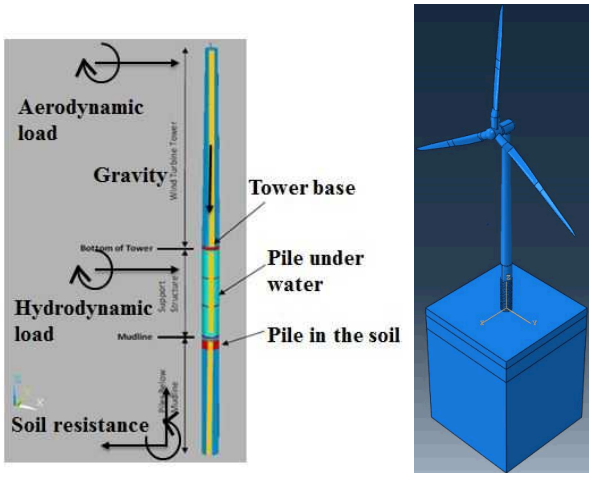

(a) (b)

Figure 6. Load analysis of the mono-pile (a) and the corresponding finite element model of the offshore wind turbine system (b).

III. Results and discussions

In this section, results from aerodynamic, hydrodynamic and structural simulations are presented and discussed. The soil-foundation interaction is analyzed using the finite element method under complex aero-hydro loading from CFD simulations.

A. Results from aerodynamic simulation

A.1. Power extraction efficiency

In this case, the wind speed is uniform at 9 m/s and the rotor speed is 1.08 rad/s. By finding out the aerodynamic torque and rotor speed from our simulation we can calculate the power extracted from the wind by the rotor. It is calculated as

$$P = T_f \dot{\theta} \approx 2.927MW.$$

The maximum power that a horizontal wind turbine can extract according to the Betz law for this rotor is

$$P_{max} = \frac{16}{27}\frac{\rho A||v_{in}||^3}{2} \approx 3.288MW.$$

From this we can conclude that the aerodynamic efficiency at the simulated wind conditions is

$$\frac{\mathrm{P}}{P_{max}} \approx 89.02\%.$$

This value is very similar to the reference value from NREL [27] and other CFD simulations [36].

A.2. Flow fields analysis

The iso-vorticity field colored with velocity magnitude is displayed in Figure 7. Therein, the wake structures after the blade and hub can be clearly seen. The air pressure distribution over the rotor surface is analyzed and plotted in Figure 8. The pressure contour is plotted on both pressure and suction side of the rotor. As expected, zone of low pressure is observed on the suction side of the blade, especially in the near-

tip region. It is the large pressure suction that creates the desired lift.

Sectional profiles of velocity contours at the stationary frame are plotted in Figure 9 for different sectional planes behind the turbine surface to understand the 3D effects on the wake region of the turbine. High-speed flow trailing from the blade tips is readily observed.

The histories of aerodynamic moments in three directions for one blade are presented in Figure 10. From the zoom-in view of the moment in the y direction, it is clear that there exist small, high-frequency fluctuations in the moment due to unsteady effects.

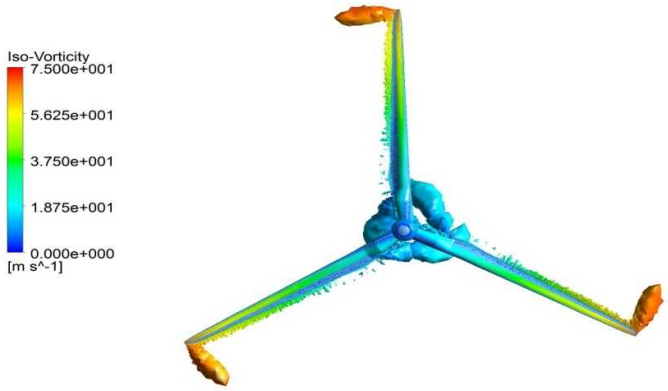

Figure 7. Iso-vorticity-magnitude surfaces colored by velocity magnitude.

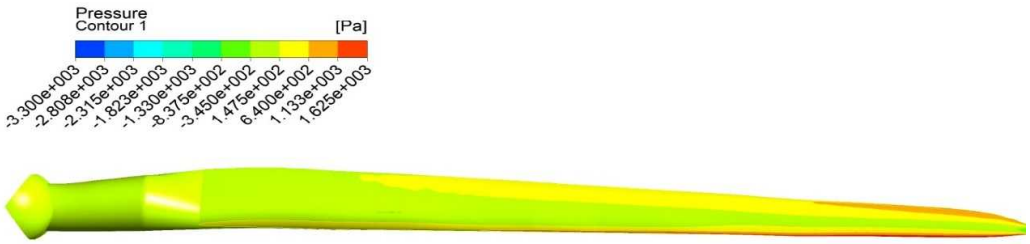

(a)

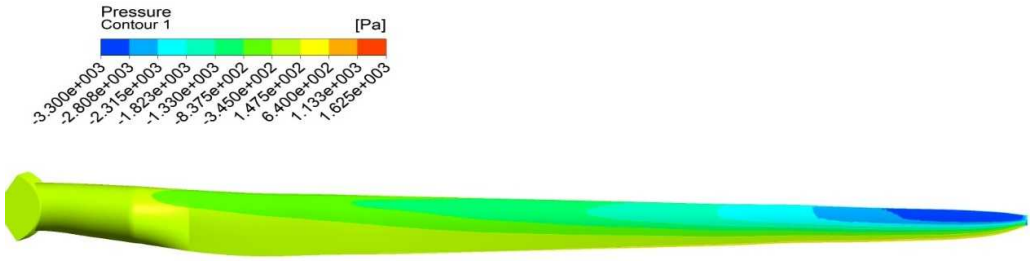

(b)

Figure 8. Pressure distribution on (a) the pressure side and (b) the suction side of the rotating blade.

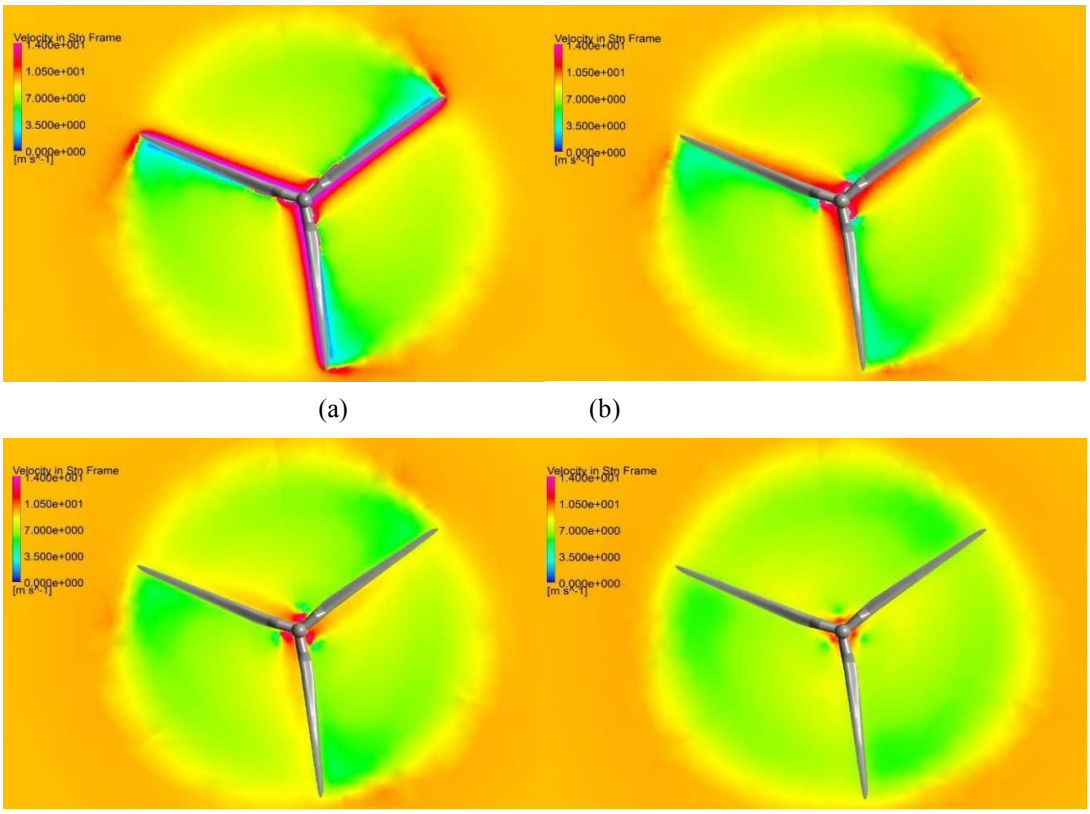

(a) (b)

(c) (d)

Figure 9. Velocity magnitude contour plots at 1, 3, 5 and 9m behind the turbine. We note that the rotor plane velocities range up to 72m⁄s but the coloring range is only up to 14m⁄s to provide more contrast.

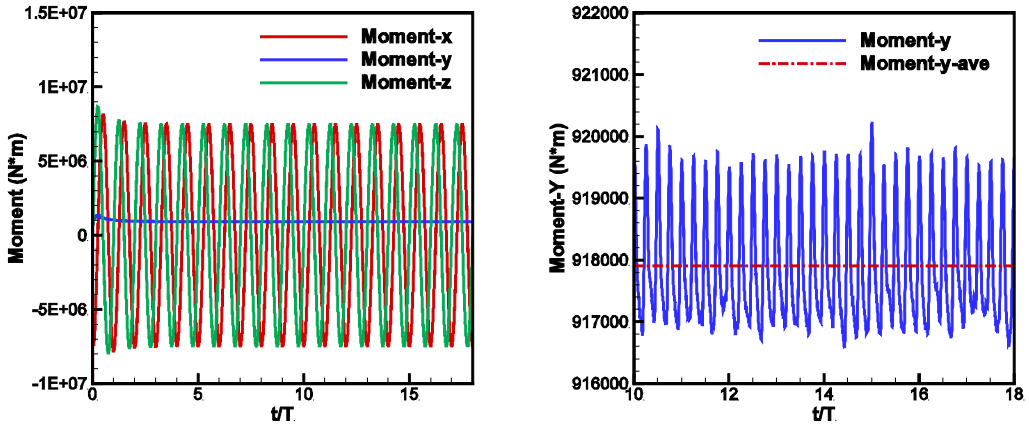

(a) (b)

Figure 10. (a) The histories of aerodynamic moments in three directions for one blade. Note that the free stream comes in the y direction. (b) A zoom-in view of the aerodynamic moment in the y direction. The average moment in the y direction is also plotted in this figure.

B. Results from hydrodynamic simulation

In this simulation, two different mesh are tested. One has 1,178,084 elements with 20 mesh grid layers around the mono pile. The other has 2,677,976 elements with 80 mesh grid layers around the mono pile. The mean drag coefficients $\bar{C}_d$ calculated from four time periods for both meshes are presented in Table 5.

Table 5. Mean drag coefficient in four periods

Coarse Mesh (1,178,084)	0.1853
Refined Mesh (2,677,976)	0.1706

In this case, the wave height is set as 4 m. The computational results from the hydrodynamic simulation are displayed in Figure 11. In this figure, the sea level, the pressure distribution on the mono-pile, and the water/air volume fraction are shown.

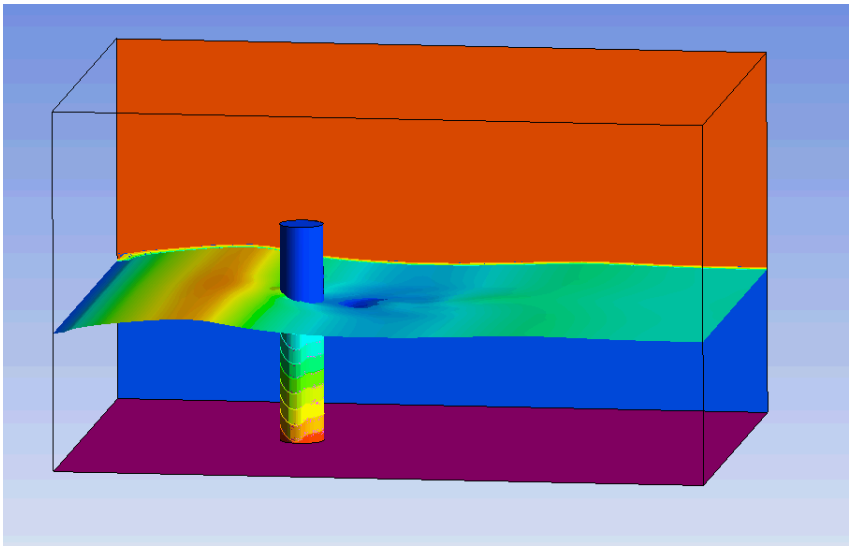

Figure 11. The sea level, the pressure distribution on the mono-pile, and the water/air volume fraction from the hydrodynamic simulation. The wave is generated via the solitary wave theory.

The sea level contour ranges from 18 m to 22m. It is clear that near the bottom of the mono-pile, the static water pressure dominates the force distribution. The wave loading can add unsteady effects onto the pressure distribution. Near the air-sea interface, the wave generates unsteady hydrodynamic loading on the mono-pile. IT is also observed that the current exerts almost constant loading on the mono-pile on the windward side. The evolution of pressure on the mono-pile in one wave period is displayed in Figure 12. In Figure 13, the pressure distribution on the mono-pile under different wave heights is displayed. It is observed that the pressure distribution on the mono pile can be significantly changed when the wave height varies.

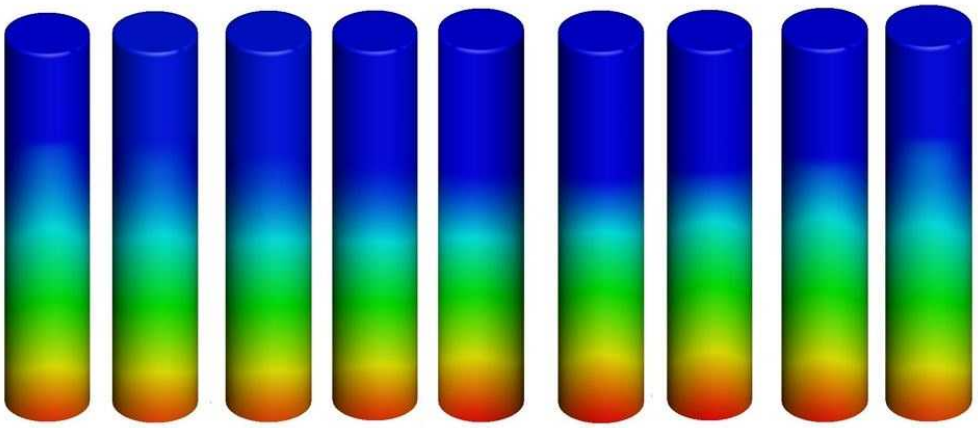

Figure 12. Pressure on the mono pile during a wave period.

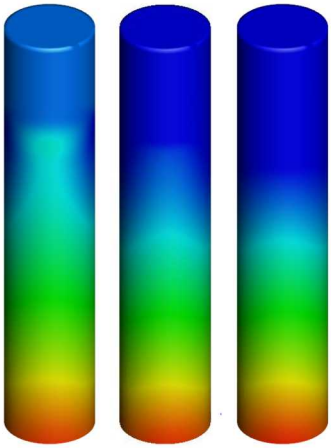

Figure 13. Static pressure distribution on the mono pile at the same time instant when wave height is 7 m, 4 m, and 1 m.

The water velocity magnitude when the wave height is 4 m is shown in Figure 14. The shape of the wave and can be clearly seen in this figure. In this case, the velocity magnitude of the water particle in x direction consists of two parts: one is the uniform current velocity which is 3 m/s, the other is the velocity driven by wave movement, which can be expressed by the following equation [37]:

$$\text{Horizontal Water Particle Velocity: } u = a\omega \frac{\cosh\left(kz + kd\right)}{\sinh(kd)} \cos(kx - \omega t)$$

Herein, a is the amplitude of the wave, ω is the wave frequency, k is the wave number, x is the horizontal coordinate, z is the vertical coordinate, and t is the time. For a given wave, a, k, d, and ω are constant.

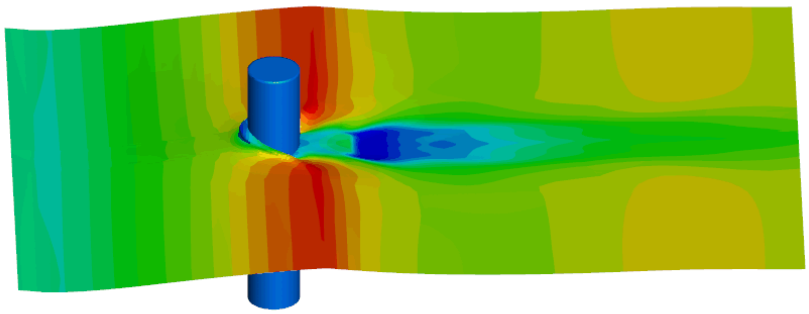

Figure 14. The velocity magnitude in x direction on the water surface when the wave height is 4 m.

In this equation, $\mathrm{acos}(kx - \omega t) = \eta$ indicates the wave displacement, or the displacement of the water surface, which has the largest positive value on the wave crest as well as the vertical coordinate z. Therefore, the horizontal particle velocity would reach its maximum magnitude on the wave crest.

In Figure 15, drag coefficient histories for both coarse and fine meshes are shown. The hydrodynamic forces from the refined mesh will be used in the structural analysis of the mono-pile foundation.

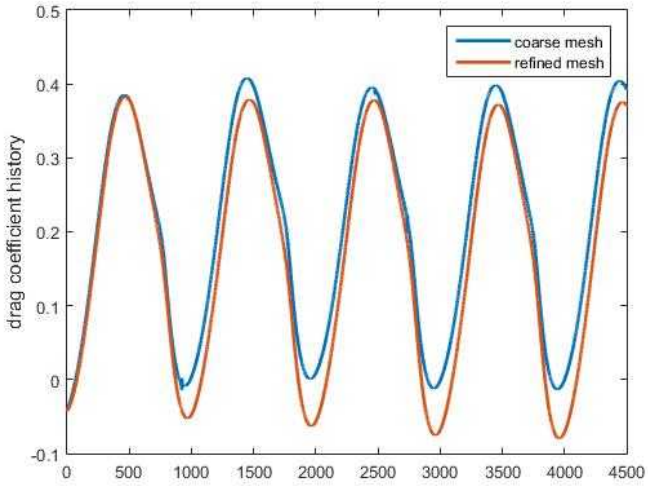

Figure 15. Drag coefficient histories in this simulation when wave height is 4 m. The x abscissa stands for the iteration steps.

C. Structural analysis of foundation

To ensure that the foundation will not fail under the loads applied, the stress field of the foundation is investigated. Figure 16 shows the Mises Stress field over 5 seconds starting at t=10s. The time history of the Mises and principle stress of foundation at the soil-water interface and of the soil at the base of the foundation were extracted. The locations in direction of the wind (labeled Up Wind and Down Wind) and those perpendicular to wind direction (Right Side and Left Side) are shown in Figure 17. The Mises stresses of the foundation and soil under the Morrison equation hydrodynamic loads are shown in Figure 18 and 19, respectively.

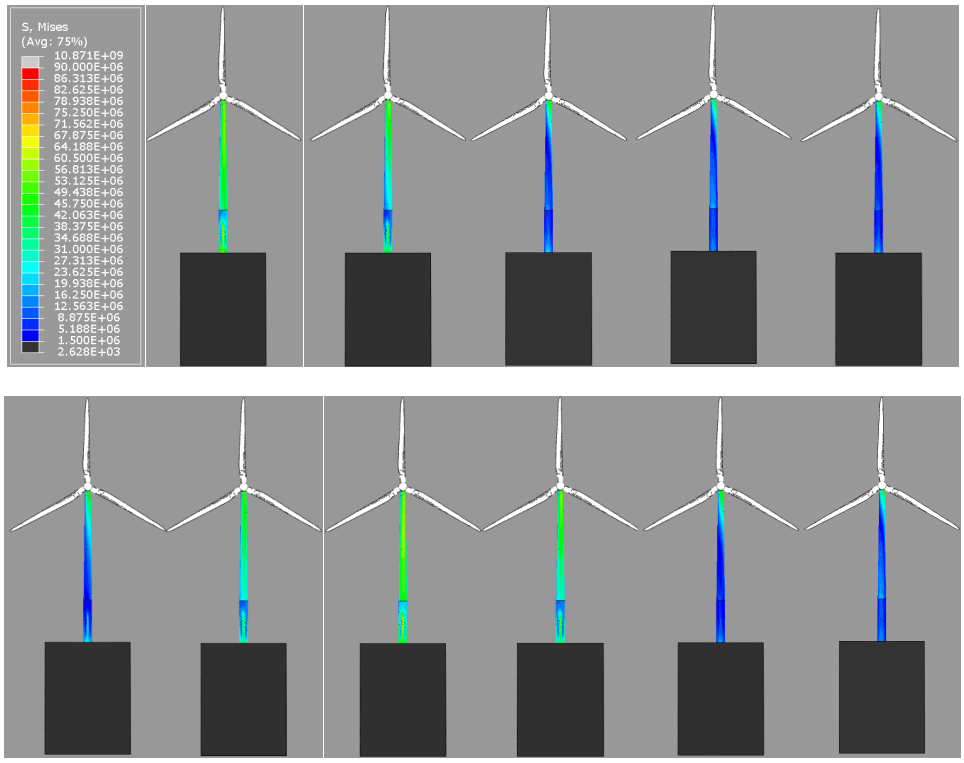

Figure 16. Mises Stress field over 5s of the tower and foundation under Morrison equation hydrodynamic load.

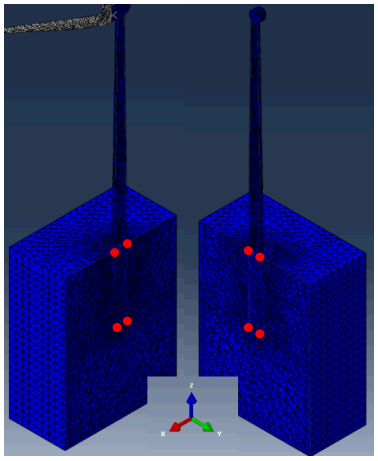

Figure 17. Locations of the elements used to extract the stress time history; in the wind direction (left) and perpendicular direction (right) of the foundation and soil.

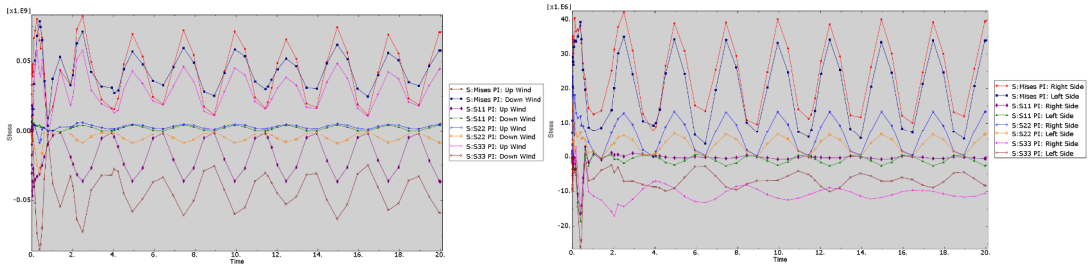

(a) (b)

Figure 18. Foundation stress histories under Morrison equation hydrodynamic loading, in the wind direction (a) and perpendicular direction (b).

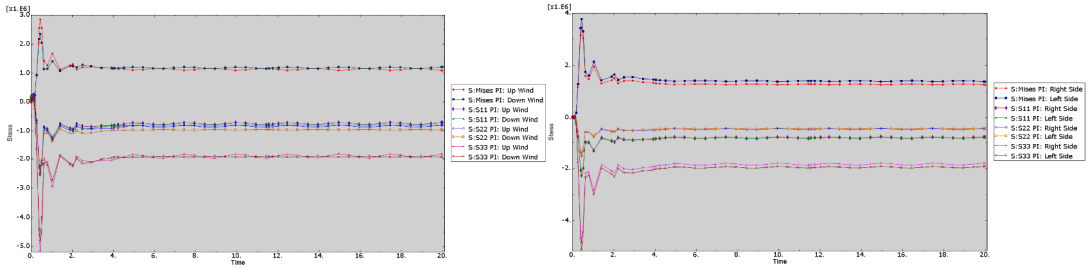

(a) (b)

Figure 19. Soil stress histories under Morrison equation hydrodynamic loading, in the wind direction (a) and perpendicular direction (b).

The stress of the system reaches the maximum value in the first second of simulation. This is consistent with the forces suddenly being applied to the system. The stresses in the foundation at the Up wind and Down wind locations have a maximum principle stress amplitude around 65 MPa and are cyclically varying. The Right side and Left side of the foundation do not experience as great of stress, because the majority of the load is in the flow direction which causes the side points to be along the neutral axis. The maximum stress of the foundation is around 79 MPa with a theoretical maximum value around 250 MPa, meaning that a safety factor of 3 is achieved.

The stresses in the soil have similar spikes within the first second as those for the foundation. These spikes are caused by the static aerodynamic forces and moments suddenly being applied. The Right and Left sides in the soil have a higher maximum stress than the Up wind and Down wind locations. This is due to the moment of the turbine applying a greater stress at the bottom of the foundation than at the top of the soil. The maximum stress in the perpendicular locations are about 0.9 MPa greater than those in the flow direction. The stress levels of the soil are lower than the bearing pressure of the soil (calculated using equations in Ref. [38]) of 8.6 MPa, since the tower is mostly supported by the friction along the length of the foundation.

The foundation was then simulation with aero-hydrodynamic loads from CFD simulations. Figure 20 shows the Mises Stress field over 5 seconds starting at t=10s. The time history of the Mises and principle stresses at the locations shown in Figure 17 were extracted. They are shown in Figures 21 and 22.

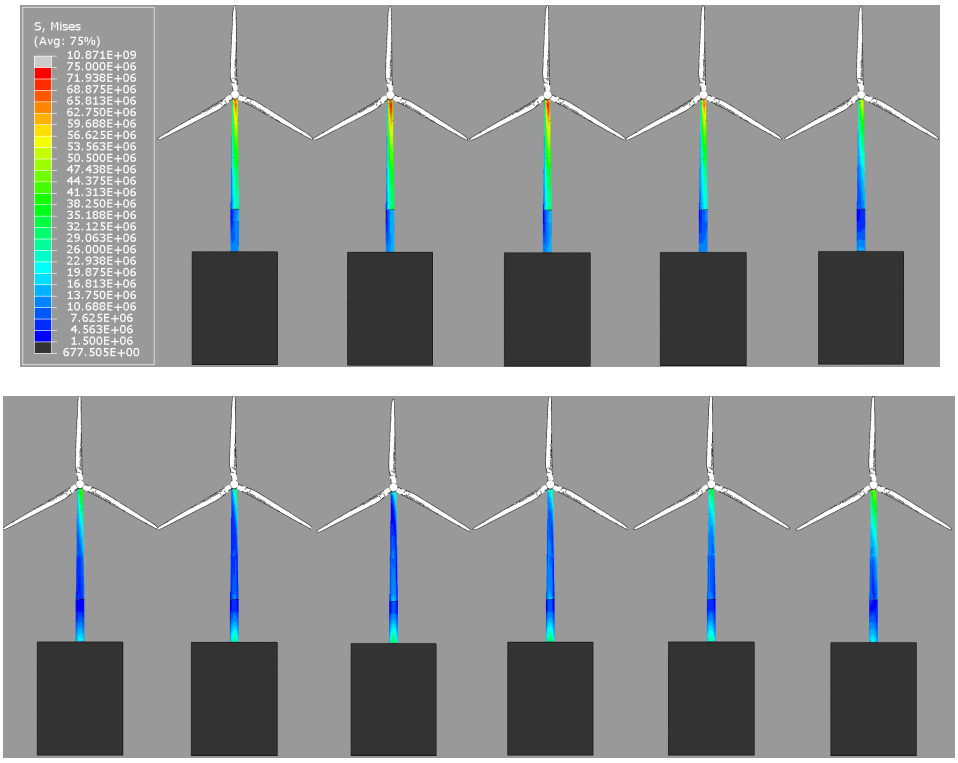

Figure 20. Mises Stress field over 5s of the tower and foundation under aero-hydrodynamic loads

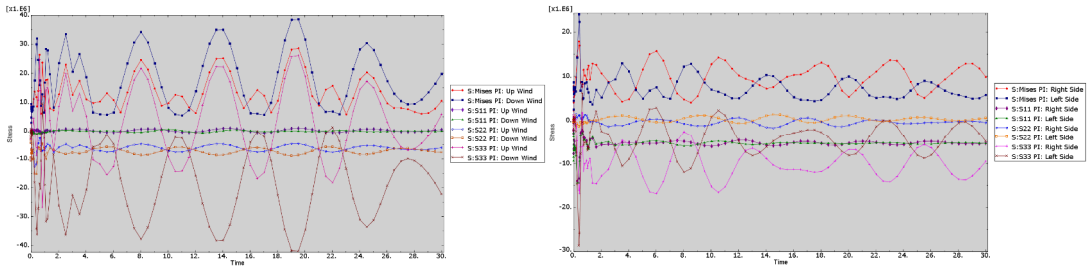

(a) (b)

Figure 21. Foundation stress histories under aero-hydrodynamic loading, in the wind direction (a) and perpendicular direction (b).

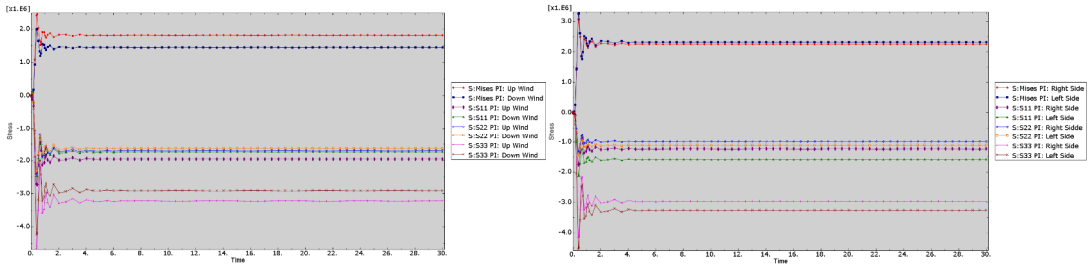

(a) (b)

Figure 22. Soil stress histories under aero-hydrodynamic loading, in the wind direction (a) and perpendicular direction (b).

The foundation Mises stresses using the hydrodynamic wave simulation were lower compared to those from the Morrison equation. The lower stresses could be from the Morrison equation being equally applied along the submerged section of the foundation; whereas the forces from the wave simulation accounts for viscosity. The stress on the foundation is also has a beat frequency because the loads do not have the same frequency and phase; where the Morrison equation has the same forcing function at each point where it is applied. The stress later in the time history is slightly higher than those when the static forces and moments are applied suddenly at the start. The stresses in the soil are higher at later time though is still much lower than the bearing pressure of the soil. It can be seen in all of the time histories that the Principle stress values have different magnitudes. This is because bending loads apply greater stresses in the axial direction (z-axis for simulation) due to the compression and tension of the part. The Mises stress is greater than all of them because it is combination of the principle stresses.

The overall stress level of the wave simulation is lower than that of the Morrison equation. To overdesign the foundation the Morrison equation would be the one to use. However, over designing the foundation will result in a cost increase of the foundation and installation.

IV. Conclusions

A comprehensive aero-hydro-structural analysis is conducted for a 5-MW offshore wind turbine system towards cost-effective deployment of offshore wind turbines in Maryland. Considering the wind turbine size and hydrological characteristics, the mono-pile foundation design is selected for current study. The aerodynamic loading for the 5-MW wind turbine rotor defined by NREL is obtained by simulating RANS equations with the Spalart-Allmaras turbulence model. The power output agrees well with the NREL reference value under the same flow conditions. The hydrodynamic loading on the foundations is evaluated by simulating the air-sea-foundation system using the VOF multiphase model. The RANS equations with the $k-\omega$ turbulence model are solved. The soil-foundation interaction under complex aero-hydro loading is then analyzed to provide a suitable foundation design with a high safety factor and minimal cost per unit energy. Specifically, the safety factor of the foundation and the soil stress are estimated via the structural analyses. Results from the mono-pile analyses indicate that the current foundation design can effectively resist the complex offshore aero-hydro loading.

Reference

[1] W. Musial and S. Butterfield, "Future for offshore wind energy in the United States: preprint," NREL/CP-500-36313, National Renewable Energy Laboratory, Golden, CO, 2004.

[2] W. Musial and B. Ram, "Large-scale offshore wind power in the United States: assessment of opportunities and barriers," NREL/TP-500-40745, National Renewable Energy Laboratory, Golden, CO, 2010.

[3] W. Musial, S. Butterfield and B. Ram, "Energy from offshore wind," NREL/CP-500-39450, National Renewable Energy Laboratory, Golden, CO, 2006.

[4] "A national offshore wind strategy: creating an offshore wind energy industry in the United States," U.S. Department of Energy, Office of Energy Efficiency and Renewable Energy, Wind & Water Power Program; U.S. Department of the Interior, Bureau of Ocean Energy Management, Regulation, and Enforcement, 2011.

[5] S. Sheng, "Report on wind turbine subsystem reliability - a survey of various databases," NREL/PR-5000-59111, National Renewable Energy Laboratory, Golden, CO, 2013.

[6] S. Malhotra, "Selection, design and construction of offshore wind turbine foundations," in *Wind Turbines*, I. Al-Bahadly, Ed., InTech, 2011, pp. 231-264.

[7] J. G. Leishman, Principles of helicopter aerodynamics, New York, NY: Cambridge University Press, 2000.

[8] D. A. Peters and C. J. He, "Correlation of measured induced velocities with a finite-state wake model," *Journal of the American Helicopter Society,* vol. 36, pp. 59-70, 1991.

[9] D. C. Quarton, "The evolution of wind turbine design analysis - a twenty year progress review," *Wind Energy,* vol. 1, pp. 5-24, 1998.

[10] P. Passon, "State-of-the-art and development needs of simulation codes for offshore wind," in *Copenhagen Offshore Wind Energy Conference*, Copenhagen, DK, 2005.

[11] C. Butterfield, W. Musial and J. Jonkman, "Overview of offshore wind technology: preprint," NREL/CP-500-42252, National Renewable Energy Laboratory, Golden, CO, 2007.

[12] R. Damiani, J. Jonkman, A. Robertson and H. Song, "Assessing the importance of nonlinearities in the development of a substructure model for the wind turbine CAE tool FAST," in *The 32nd International Conference on Ocean, Offshore and Arctic Engineering*, Nantes, France, 2013.

[13] J. G. Leishman, "Challenges in modeling the unsteady aerodynamics of wind turbines," in *the 21st ASME Wind Energy Symposium and the 40th AIAA Aerospace Sciences Meeting*, Reno, NV, 2002.

[14] L. J. Vermeer, J. Sørensen and A. Crespo, "Wind turbine wake aerodynamics," *Progress in Aerospace Sciences,* vol. 39, pp. 467-510, 2003.

[15] M. O. L. Hansen, J. N. Sørensen, S. Voutsinas, N. Sørensen and H. A. Madsen, "State of the art in wind turbine aerodynamics and aeroelasticity," *Progress in Aerospace Sciences,* vol. 42, pp. 285-330, 2006.

[16] J. M. Jonkman and M. L. J. Buhl, "FAST User's Guide," NREL/EL-500-38230, National Renewable Energy Laboratory, Golden, Co, 2005.

[17] A. R. Henderson, M. B. Zaaijer and T. R. Camp, "Hydrodynamic loading on offshore wind turbines," in *Offshore Wind Energy in Mediterranean and Other European Seas (OWEMES conference)*, Naples, Italy, 2003.

[18] M. A. Chella, A. Tørum and D. Myrhaug, "An overview of wave impact forces on offshore wind turbine substructures," *Energy Procedia,* vol. 20, pp. 217-226, 2012.

[19] H. G. Poulos and E. H. Davis, Pile foundation analysis and design, Wiley, 1980.

[20] P. Cuéllar, Pile foundations for offshore wind turbines: numerical and experimental investigations on the behavior under short-term and long-term cyclic loading, Berlin, Germany: Berlin Institute of Technology, 2011.

[21] B. Broms, "Lateral resistance of piles in cohesionless soils," *ASCE Journal of the Soil Meachanics and Foundations Division,* vol. 90, pp. 123-156, 1964.

[22] M. Novak, "Dynamic stiffness and damping of piles," *Canadian Geotechnical Journal,* vol. 11, pp. 574-598, 1974.

[23] G. Gazetas and N. Makris, "Dynamic pile-soil-pile interaction. Part I: analysis of axial vibration," *Earthquake Engineering & Structural Dynamics,* vol. 20, pp. 115-132, 1991.

[24] N. Makris and G. Gazetas, "Dynamic pile-soil-pile interaction. Part II: lateral and seismic response," *Earthquake Engineering & Structural Dynamics,* vol. 21, pp. 145-162, 1992.

[25] M. Yuan, J. H. Ding and Q. Zhang, "Analysis of spatial effects of two-row pile structure of foundation pit based on elastic resistance method," *International Journal of Civil & Environmental Engineering,* vol. 11, p. 134, 2011.

[26] I. Chowdhury and S. P. Dasgupta, Dynamics of structure and foundation - a unified approach, New York: CRC Press, 2009.

[27] J. Jonkman, S. Butterfield, W. Musial and G. Scott, "Definition of a 5-MW reference wind turbine for offshore system development," NREL/TP-500-38060, National Renewable Energy Laboratory, Golden, CO, 2009.

[28] G. G. Stokes, "On the theory of oscillatory waves," *Transactions of the Cambridge Philosophical Society,* vol. 8, pp. 441-455, 1847.

[29] TSUCHIYA, Yoshito; YASUDA, Takashi, "A New Approach to Stokes Wave Theory," vol. 31, no. 1981-03, 1981.

[30] T. Hedges, "Regions of validity of analytical wave theories," in *Proceedings of the Institution of Civil Engineers.* , 1995.

[31] "Ocean Surface Currents (OSCAR)," NASA, [Online]. Available: http://oceanmotion.org/html/resources/oscar.htm. [Accessed 19 11 2015].

[32] O. S. A. Ahmed, "Vertical dynamic soil-pile interaction for machine foundations," Ph. D. thesis, University of Maryland, 2015.

[33] E. L. Wilson, Three dimensional static and dynamic analysis of structures: A physical approach with emphasis on earthquake engineering, Berkley: Computers and Structures, 2002.

[34] F. V. D. Blasio, Introduction to the physics of landslides: Lecture notes on the dynamics of mass wasting, Springer Science, 2011.

[35] J. M. J. Journee and W. W. Massie, Offshore hydromechanics, Delft University of Technology, 2001.

[36] Y. Bazilevs, M.-C. Hsu, I. Akkerman, S. Wright, K. Takizawa, B. Henicke, T. Spielman and T. E. Tezduyar, "3D simulation of wind turbine rotors at full scale. Part I: Geometry modeling and aerodynamics," *International Journal for Numerical Methods in Fluids,* vol. 65, pp. 207-235, 2011.

[37] D. M. Sheppard, "Regular Ocean Waves," [Online]. Available: http://www.essie.ufl.edu/~sheppard/OCE3016/Ocean%20Waves.pdf. [Accessed 2 12 2015].

[38] S. K. Prasad, Bearing capacity of soil, S.J. College of Engineering, Mysore, 2013.